

Obesity-Induced Inflammation Is Associated with Alterations in Subcellular Zinc Pools and Premature Mammary Gland Involution in Lactating Mice^{1–3}

Stephen R Hennigar,⁴ Vanessa Velasquez,⁴ and Shannon L Kelleher^{4,5*}

⁴Department of Nutritional Sciences, The Pennsylvania State University, University Park, PA; and ⁵Departments of Cell and Molecular Physiology, Pharmacology, and Surgery, Penn State Hershey College of Medicine, Hershey, PA

Abstract

Background: Lactation failure is common in overweight and obese women; however, the precise mechanism remains unknown.

Objective: We tested the hypothesis that obesity-induced inflammation in the mammary gland (MG) redistributes subcellular zinc pools to promote cell death of mammary epithelial cells (MECs) and premature involution.

Methods: Female DBA/2J mice were fed a high-fat (obese; 45% kcal from fat, $n = 60$) or control diet (lean; 10% kcal from fat, $n = 50$) for 5 wk and bred. MG cytokines and macrophage infiltration were determined by reverse transcriptase-polymerase chain reaction and F4/80 staining, respectively. Zinc concentration was analyzed by atomic absorption spectroscopy, and zinc transporters and markers of endoplasmic reticulum (ER) stress, autophagy, and involution were measured by immunoblot. To confirm effects of inflammation, tumor necrosis factor- α (TNF) or vehicle was injected into adjacent MGs of lean lactating C57BL/6 mice ($n = 5$) and cultured MECs (HC11 cells) were treated with TNF in vitro.

Results: Seventy-seven percent of obese mice failed to lactate (lean: 39%; $P < 0.001$). Obese mice capable of lactating had greater macrophage infiltration (obese: 135 ± 40.4 macrophages/mm²; lean: 63.8 ± 8.9 macrophages/mm²; $P < 0.001$) and elevated TNF expression ($P < 0.05$), concurrent with lower zrt-irt-like protein 7 abundance ($P < 0.05$) and higher ER zinc concentration (obese: 0.36 ± 0.004 $\mu\text{g Zn/mg protein}$; lean: 0.30 ± 0.02 $\mu\text{g Zn/mg protein}$; $P < 0.05$) compared with lean mice. Heat shock protein 5 (HSPA5) expression ($P < 0.05$) was suppressed in the MG of obese mice, which was consistent with HSPA5 suppression in TNF-injected MGs ($P < 0.01$) and MECs treated with TNF in vitro ($P < 0.01$). Moreover, obesity increased lysosomal activity ($P < 0.05$) and autophagy in the MG, which corresponded to increased zinc transporter 2 abundance and lysosomal zinc concentration compared with lean mice (obese: 0.20 ± 0.02 $\mu\text{g Zn/mg protein}$; lean: 0.14 ± 0.01 $\mu\text{g Zn/mg protein}$; $P < 0.05$). Importantly, MGs of obese mice exhibited markers of apoptosis ($P = 0.05$) and involution ($P < 0.01$), which were not observed in lean mice.

Conclusions: Diet-induced obesity created a proinflammatory MG microenvironment in mice, which was associated with zinc-mediated ER stress and autophagy and the activation of premature involution. *J Nutr* 2015;145:1999–2005.

Keywords: lactation, TNF, zinc transporter, ZnT2, ZIP7

Introduction

Over one-third of women of reproductive age are overweight (BMI: 25–29 kg/m²) or obese (BMI: ≥ 30 kg/m²) (1). Being overweight or obese impairs mammary gland (MG)⁶ function and compromises the ability to initiate and maintain lactation

[reviewed by Jevitt et al. (2), Rasmussen (3), and Stuebe et al. (4)]; however, the biological mechanisms responsible for the lactation defects in obese women are not well understood.

¹ Supported in part by funds from the NIH (HD058614 to SLK and HD05614-S1 to VV).

² Author disclosures: SR Hennigar, V Velasquez, and SL Kelleher, no conflicts of interest.

³ Supplemental Figures 1 and 2 and Supplemental Tables 1–4 are available from the “Online Supporting Material” link in the online posting of the article and from the same link in the online table of contents at <http://jn.nutrition.org>.

* To whom correspondence should be addressed. E-mail: slk39@psu.edu.

⁶ Abbreviations used: *Actb*, β -actin; CSF, macrophage colony stimulating factor; *Csf1*, colony-stimulating factor 1; ER, endoplasmic reticulum; H&E, hematoxylin and eosin; HSPA5, heat shock protein 5; IRE-1, inositol-requiring 1; KAR2, karyogamy 2; LAMP1, lysosome-associated membrane protein 1; LC3, microtubule-associated protein light chain 3; LD, lactation day; MCP-1, monocyte chemoattractant protein 1; MEC, mammary epithelial cell; MG, mammary gland; p-STAT3, phosphorylated signal transducer and activator of transcription 3; *Tnf*, tumor necrosis factor- α ; t-STAT3, total signal transducer and activator of transcription 3; UPR, unfolded protein response; v-ATPase, vacuolar H⁺-ATPase; ZIP7, zrt-irt-like protein 7; ZnT2, zinc transporter 2.

Adipocytes secrete a number of proinflammatory cytokines, including IL-6, IL-1 β , and monocyte chemoattractant protein 1 (MCP-1). Indeed, greater TNF and IL-6 expression is detected in the MGs of obese rats (5). Both TNF and MCP-1 act as chemoattractants for macrophage recruitment (6), which, in turn, secrete cytokines such as IL-6, TNF, and colony-stimulating factor 1 (CSF1) (7), perpetuating the proinflammatory phenotype. This is particularly relevant because TNF has been shown to activate postlactational involution (8, 9). Furthermore, both lactation (10) and obesity (11) create physiologic states of enhanced endoplasmic reticulum (ER) stress. ER stress signaling sets into motion the short-term cytoprotective mechanism of the unfolded protein response (UPR), which coordinates attenuation of protein translation with an increase in the lysosomal-degradation pathway known as macroautophagy (here referred to as autophagy) and the ER-associated degradation pathway to protect against cell death (12, 13). With prolonged ER stress, the UPR declines and apoptotic mechanisms are activated (14). Thus, mammary epithelial cells (MECs) can effectively manage the ER stress and autophagy inherent to lactation but the added physiologic stress of obesity may tip the cellular phenotype toward death.

Alterations in subcellular zinc pools may underlie the activation of autophagy, ER stress, and cell death. Zinc accumulation in lysosomes activates autophagy in cultured neurons (15) and lysosomal-mediated cell death in MECs (9). Zinc transporter 2 (ZnT2) normally imports zinc into secretory vesicles during lactation (16) and is not found in lysosomes in the MGs of nulliparous or lactating mice or MECs (16, 17). However, we recently found that TNF redistributes ZnT2 to accumulate zinc in lysosomes and activates lysosomal-mediated cell death of MECs during the initial phase of MG involution (9). In addition, depletion of ER zinc activates ER stress (18–20), and loss-of-function mutations in the ER zinc exporter *Catsup* [human zrt-irt-like protein 7 (ZIP7) homolog] impairs secretory trafficking and activates cell death (21). Here, we tested the hypothesis that the proinflammatory microenvironment in the obese MG alters ER and lysosomal zinc pools, resulting in secretory defects, cell death, and premature involution.

Methods

Mouse husbandry. This study was approved by the Institutional Animal Care and Use Committee at The Pennsylvania State University, which is accredited by the Association for Assessment and Accreditation of Laboratory Animal Care International. All mice were housed individually in polycarbonate cages, had free access to feed and water, and were maintained on a 12-h light/dark cycle under controlled temperature and humidity.

Mouse model of diet-induced obesity. Male and female DBA/2J mice were obtained commercially (Jackson Laboratories) at 3 wk of age. At 4 wk of age female mice were randomly assigned to either a high-fat (45% kcal from lard, $n = 60$) or control (10% kcal from lard, $n = 50$) diet (D12451 and D12450B, respectively; Research Diets, Inc.). The diets were similar in composition except for fat and carbohydrate content (Supplemental Table 1) and are commonly used to generate a diet-induced obesity model (22–25). Mice fed the high-fat diet were defined as diet-induced obese once their body weight was >2 SDs above the mean of the control diet-fed group ($\sim 20\%$ heavier) (26). Female mice were mated and allowed to deliver naturally. Mice were fed their respective diets during pregnancy until lactation day (LD) 5. Feed intake and body weight were measured weekly. Litters were weighed and the number of pups per litter was counted on the day of birth and at LD 5. The study was terminated during early lactation because of the substantial degree of litter loss that occurred in this diet-induced obesity model.

TNF-injected mice. Mice were bred and litters were maintained at 6 pups/dam. TNF (R&D Systems) was injected into MGs of lactating mice ($n = 5$) as described previously (8, 9).

Cell culture. Mouse MECs (HC11) were a gift from Jeffrey Rosen (Baylor College of Medicine, Houston, Texas) and were used with permission of Bernd Groner (Institute for Biomedical Research, Frankfurt, Germany). Cells were maintained as described previously (9). To differentiate HC11 cells into a secretory phenotype, cells were cultured in differentiation medium (serum-free growth medium without epidermal growth factor supplemented with 1 $\mu\text{g}/\text{mL}$ prolactin and 1 μM cortisol) for 24 h at 37°C. After differentiation, cells were pretreated with zinc sulfate (10 μM) for 3 h in growth medium followed by incubation with or without TNF (15 $\mu\text{g}/\text{L}$) for 24 h in serum-free medium at 37°C.

Milk secretion. Milk secretion was measured in lean and obese mice ($n = 5$ –6 mice/group) on LD 5 using the weigh-suckle-weigh technique over 30 min (27). Mice were killed by carbon dioxide inhalation, and MGs were fixed in 4% phosphate-buffered paraformaldehyde overnight.

Milk and tissue collection. Milk was manually expressed ($n = 6$ –8 mice/group) on LD 5 (28). Mice were killed by carbon dioxide inhalation. Inguinal MGs were used for analysis. MGs used for protein analysis were frozen on dry ice and stored at -80°C until analysis. MGs used for RNA were stored in RNAlater (Sigma-Aldrich) at -20°C until analysis.

Milk protein concentration. Whole milk ($n = 6$ –8 mice/group) was centrifuged at $2000 \times g$ for 15 min at 4°C. The cream layer was scraped away using a pipette tip and the skimmed milk was transferred to a clean tube. Skimmed milk was diluted in 2 vol of buffer (50 mol/L Na_2PO_4 , 150 mmol/L NaCl, 50 mmol/L EDTA) and centrifuged twice at $11,600 \times g$ for 15 min at 4°C. Protein concentration in the supernatant was measured by Bradford assay.

Histology. Paraformaldehyde-fixed MGs ($n = 3$ mice/group) were serially dehydrated in ethanol, embedded in paraffin, and sectioned (5 μm) onto positively charged glass slides (28). Sections were stained with hematoxylin and eosin (H&E) and evaluated using immunohistochemistry (28). Sections stained with H&E were used to evaluate adipocyte number and size. The number of adipocytes in 3 random areas under $4\times$ magnification was counted and expressed as a number of adipocytes/unit area (mm^2) \pm SD. Adipocyte size was assessed by comparing maximum adipocyte diameter from H&E-stained images using the ruler tool on Photoshop. Rat anti-mouse F4/80 (macrophage marker, 1:1000; MCA497; AbD Serotech) was used for immunostaining and was detected with biotinylated goat anti-rat IgG (Vector Labs), visualized using the ABC Vectastain kit (Vector Labs), and counterstained with toluidine blue (EMD). The number of cells that stained positive for F4/80 was counted in 3 random areas under $10\times$ magnification and expressed as a mean \pm SD/unit area (mm^2). Sections were imaged using a Leica DM IL LED microscope and LAS V3.6 software (Leica Microsystems).

Real-time relative RT-PCR. MGs ($n = 7$ –8 mice/group) were homogenized in TRIzol (Sigma-Aldrich), and RNA was isolated following the manufacturer's instructions (Invitrogen). Real-time PCR was performed as previously described (16). Primer sequences were chosen using Primer3 (Whitehead Institute for Biomedical Research; Supplemental Table 2), and specificity was validated by assessment of single temperature dissociation peak (data not shown). Each sample was measured in duplicate and normalized to β -actin (*Actb*). Data were expressed as fold of the lean group (mean \pm SD).

Subcellular fractionation. Crude membrane proteins (29) and subcellular fractions (30) were isolated as described previously.

Acid phosphatase activity. Acid phosphatase activity was used as an index of lysosomal activity and autophagy. Activity was measured using a commercially available kit (CS0740; Sigma-Aldrich) as described previously (9).

Immunoblotting. Proteins (~30 µg) prepared as described previously were electrophoresed and immunoblotted (9, 16). Antibodies used for immunoblotting were as follows: heat shock protein 5 (HSPA5; also known as BiP/GRP78; 1:1000; #3177; Cell Signaling), calnexin (1:1000; ab22595; Abcam), caspase-3 (1:1000; #9665; Cell Signaling), lysosome-associated membrane protein 1 (LAMP1; 1:1000; ab24170; Abcam), microtubule-associated protein light chain 3 (LC3; 1:1000; #4108; Cell Signaling), phosphorylated signal transducer and activator of transcription 3 (p-STAT3; 1:1,000; #9145, Cell Signaling), succinate dehydrogenase (1:1000; ab14715; Abcam), vacuolar-type H⁺-ATPase (v-ATPase; 1:500; A00938-40; GenScript), ZIP7 (1:1000; ab137226; Abcam), and ZnT2 (1 µg/mL) (28). Antibodies were detected with donkey anti-rabbit IgG-HRP (1–25,000; GE Healthcare) or IRDyes (1:20,000; LiCor). Membranes were stripped and reprobed for β-actin (1:5000; A5441; Sigma-Aldrich) and detected with sheep anti-mouse IgG-HRP (1:10,000; GE Healthcare) or IRDyes (1:20,000; LiCor). Proteins were visualized with Super Signal West Femto or Pico Chemiluminescent Substrate (Pierce Biotechnology) and exposed to autoradiography film or imaged using an Odyssey infrared imaging system (LiCor). Relative band density was quantified using Carestream Gel Logic 212 Pro. Representative immunoblots were provided. Experiments were repeated 2–3 times and statistical analysis was performed on the signal intensity of the protein of interest relative to β-actin (or LC3-I or total signal transducer and activator of transcription 3 [t-STAT3]) on all protein bands from each experiment (≥3 replicates/group).

Statistical analysis. Results are presented as means ± SDs. Statistical comparisons were performed using Student's *t* test (Prism GraphPad). χ²-Analysis (Fisher's exact test) was used to compare the number of mice able to maintain lactation. Repeated-measures ANOVA was used to compare feed intake and body weight. A significant effect of diet was demonstrated at *P* < 0.05.

Results

Diet-induced obesity suppresses the secretory capacity of the MGs. Average weekly feed intake was similar between lean and obese mice; however, energy intake was 20% greater (*P* < 0.0001) in obese mice because of the higher energy density of the high-fat diet (Supplemental Table 3). Obese mice were >20% heavier than mice fed the control diet after 5 wk (Supplemental Table 3). Conception rates were ~34% lower (*P* < 0.05) and litter size and offspring weight were significantly lower (*P* < 0.05) in obese mice than in lean mice (Supplemental Table 4). Furthermore, significantly more obese dams (77%) failed to nurse their offspring past LD 5 compared with lean dams (39%; *P* < 0.001), resulting in decreased survival rates of offspring from obese dams. Milk secretion did not differ between obese mice that were capable of nursing their offspring (obese lactating mice: 0.03 ± 0.01 mg of milk/dam) and lean mice capable of nursing their offspring (lean lactating mice: 0.05 ± 0.02 mg of milk/dam; *P* = 0.29). Total milk protein concentration was significantly lower in obese lactating mice (25.1 ± 1.3 g protein/L) than in lean lactating mice (32.1 ± 3.2 g protein/L; *P* < 0.001). Collectively, this suggests that obesity suppressed the secretory capacity of the MGs.

Diet-induced obesity creates a proinflammatory MG microenvironment. Consistent with previous reports (5, 31, 32), we found that obese mice displayed hallmarks of an inflammatory MG microenvironment. MG weight in obese lactating mice (0.65 ± 0.06 g) was significantly higher than MG weight in lean lactating mice (0.47 ± 0.05 g; *P* < 0.05). There was no significant difference in the mean number of adipocytes in the MGs from obese lactating mice (672 ± 86.2 adipocytes/mm²) compared with lean lactating mice (772 ± 53.8 adipocytes/mm²; *P* = 0.38).

However, adipocyte size in MGs from obese lactating mice increased by 100% relative to the adipocytes of lean lactating mice (Figure 1A). Macrophage abundance was significantly greater in MGs from obese lactating mice (135 ± 40.4 macrophages/mm²) than in MGs from lean lactating mice (63.8 ± 8.9 macrophages/mm²; *P* < 0.001). Expression of *Tnf* (*P* < 0.05), *Csf1* (*P* < 0.01), and *Il6* (*P* < 0.05) was significantly greater in MGs from obese lactating mice than in MGs lean lactating mice (Figure 1B). These studies confirmed that obesity creates a proinflammatory microenvironment in the MG.

Diet-induced obesity during lactation suppresses ER stress. To assess the effects of the obese MG microenvironment on ER stress during lactation, we first measured HSPA5 expression as a marker of ER stress. Surprisingly, we found that MGs from obese lactating mice had a significantly lower abundance of HSPA5 than MGs from lean lactating mice (*P* < 0.05), similar to the decrease in HSPA5 abundance that occurs in involuting MGs (Figure 2A). We next measured ZIP7 abundance and found that ZIP7 was slightly lower in MGs from obese lactating mice than in MGs from lean lactating mice (Figure 2B; *P* < 0.05), similar to the decreased abundance of ZIP7 that occurs in involuting MGs. Importantly, reduced ZIP7 was associated with a significant increase in the zinc concentration of ER/Golgi apparatus-enriched fractions (Supplemental Figure 1) isolated from MGs of obese lactating mice compared with identical fractions isolated from lean lactating mice (Figure 2C; *P* < 0.05). This suggests that zinc accumulates in the ER of obese MGs, which is associated with suppressed ER stress and is similar to what is observed in involuting MGs.

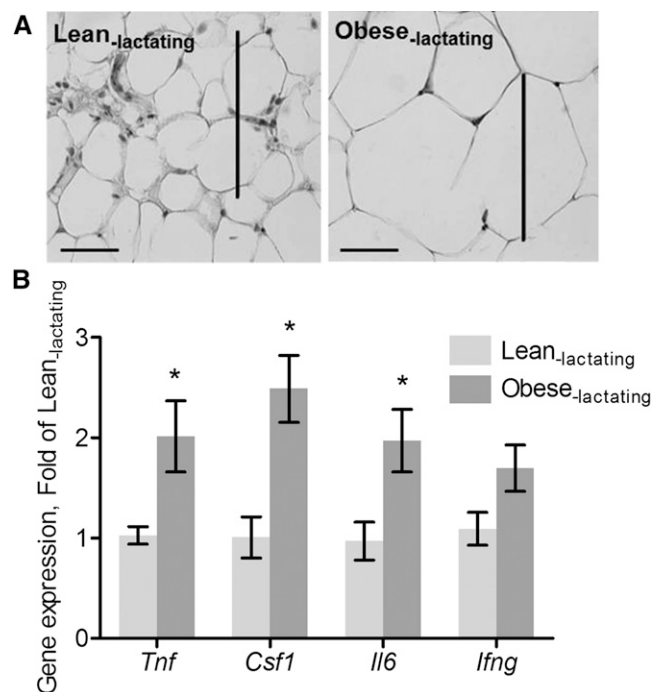
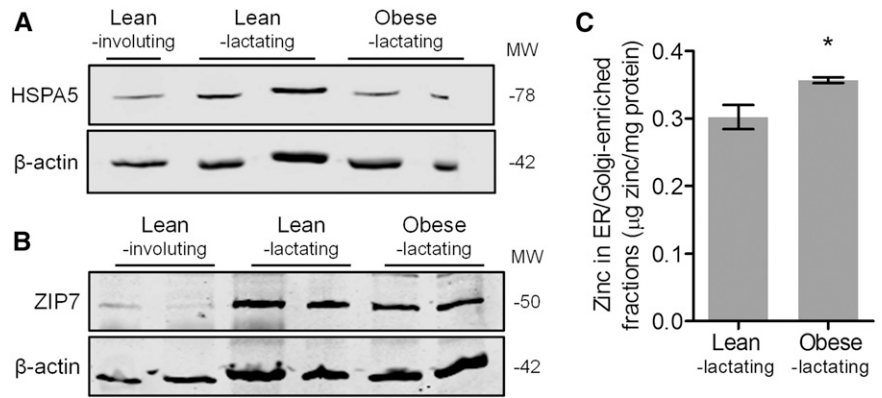


FIGURE 1 Adipocyte size and cytokine mRNA expression in MGs from lean lactating and obese lactating mice. (A) Representative images of H&E-stained sections. Adipocyte size is shown (scale bars = 100 µm). (B) Cytokine mRNA expression. Data are means ± SDs, *n* = 8 (lean lactating) or *n* = 7 (obese lactating). *Different from lean lactating mice, *P* < 0.05. *Csf1*, colony-stimulating factor; H&E, hematoxylin and eosin; *Ifng*, interferon-γ; MG, mammary gland; *Tnf*, tumor necrosis factor-α.

FIGURE 2 Markers of ER stress and zinc metabolism in MGs from lean lactating and obese lactating mice. Representative immunoblots of protein abundance of (A) HSPA5 and (B) ZIP7. β -Actin was used as a loading control. Involuting MGs from lean mice are shown for comparison. (C) Zinc concentration of fractions enriched in ER/Golgi apparatus isolated from MGs of lean lactating and obese lactating mice. Data are means \pm SDs, $n = 5$ mice/group. $*P < 0.05$. ER, endoplasmic reticulum; HSPA5, heat shock protein 5; MG, mammary gland; MW, molecular weight; ZIP7, zrt-irt-like protein 7.



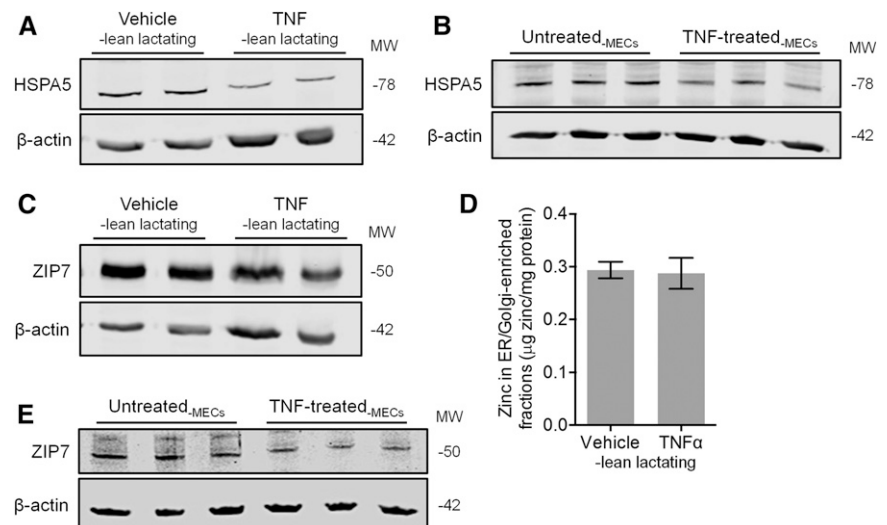
TNF partially explains discoordinated ER zinc transport in the MGs of obese mice. To determine if TNF contributes to the suppression of ER stress, we first gently injected TNF or saline into MG fat pads 4 and 9, respectively, of lean lactating mice on LD 5. Offspring were returned to the dams and offspring suckling was observed. The MGs were collected 24 h after injection, and H&E staining confirmed that TNF activated involution (8, 9). We found that HSPA5 expression was suppressed in TNF-injected MGs compared with saline-injected MGs (Figure 3A; $P < 0.01$), similar to our observations in MGs from involuting mice and obese lactating mice. To determine whether this was mediated by a direct effect of TNF on MECs, we treated MECs in vitro with TNF (15 $\mu\text{g/L}$) for 24 h. Consistent with our in vivo findings, MECs treated with TNF in vitro had significantly reduced HSPA5 abundance compared with untreated controls (Figure 3B; $P < 0.01$), suggesting that TNF mediates suppression of the UPR in MECs. We next examined whether changes in ER zinc pools were associated with this process. Although we found a slight reduction in ZIP7 abundance in TNF-injected MGs compared with saline-injected MGs (Figure 3C; $P < 0.05$), this did not affect the zinc concentration of ER/Golgi-enriched fractions (Figure 3D; $P = 0.85$). Moreover, although we detected a slight reduction in ZIP7 abundance in TNF-stimulated cells in vitro, this was not statistically significant (Figure 3E; $P = 0.11$). Collectively, this suggests that the proinvolvement signal TNF suppresses ER stress and ZIP7 abundance but that TNF is not the only factor involved in increasing ER zinc pools during involution.

Obesity during lactation enhances lysosomal activity and activates autophagy. To assess hallmarks of lysosomal activity/autophagy, we noted that obese lactating mice had increased acid phosphatase activity (Figure 4A; $P < 0.05$) (33) and v-ATPase expression (Figure 4B; $P < 0.01$) (34) compared with lean lactating mice. When autophagy is activated, the LC3-I protein found in cytosol is lipidated and inserted into the membranes of autophagosomes as LC3-II (35).

We detected greater protein abundance of LC3-II relative to LC3-I in MGs from obese lactating mice compared with lean lactating mice (Figure 4C; $P < 0.05$). Finally, MGs from obese lactating mice accumulated lipid droplets (Figure 5B), a substrate for and marker of autophagy (36). We next measured ZnT2 abundance and found that although total ZnT2 abundance was unchanged (Supplemental Figure 2), lysosome-enriched fractions isolated from obese lactating mice contained greater ZnT2 (Figure 4D; $P < 0.05$) than similar fractions isolated from lean lactating mice. Moreover, we found that these lysosome-enriched fractions also had greater zinc content (Figure 4E; $P < 0.05$) than identical fractions isolated from lean lactating mice. Collectively, this suggests that obesity during lactation is associated with a redistribution of ZnT2 and zinc to lysosomes and increased lysosomal activity and autophagy.

Obesity activates MG involution. Finally, to determine whether the decrease in ER stress and activation of autophagy observed in obese lactating mice was associated with cell death and premature involution, we measured the abundance of caspase-3

FIGURE 3 Effects of TNF on markers of ER stress and zinc metabolism in lean lactating mouse MGs in vivo and differentiated MECs in vitro. Representative immunoblots of protein abundance of HSPA5 in (A) TNF- and vehicle-injected mouse MGs in vivo and (B) HC11 MECs in vitro. (C) Representative immunoblot of protein abundance of ZIP7 in TNF- and vehicle-injected MGs. (D) Zinc concentration of fractions enriched in ER/Golgi apparatus isolated from TNF- and vehicle-injected MGs. Data are means \pm SDs, $n = 5$ mice/group. $*P < 0.05$. (E) Representative immunoblot of protein abundance of ZIP7 in HC11 MECs in vitro. β -Actin was used as a loading control. ER, endoplasmic reticulum; HSPA5, heat shock protein 5; MEC, mammary epithelial cell; MG, mammary gland; MW, molecular weight; ZIP7, zrt-irt-like protein 7.



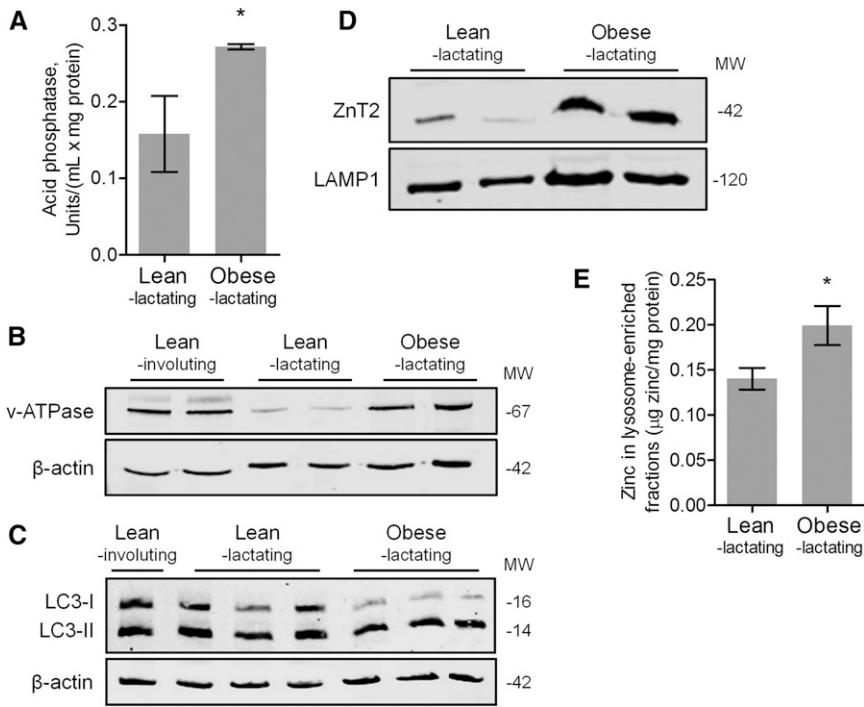


FIGURE 4 Markers of lysosomal activity/autophagy and zinc metabolism in MGs from lean lactating and obese lactating mice. (A) Data are means \pm SDs, $n = 5$ mice/group. * $P < 0.05$. Representative immunoblots of protein abundance of (B) v-ATPase and (C) LC3-I and LC3-II in MGs from lean lactating and obese lactating mice. Involuting MGs from lean mice are shown for comparison. (D) Representative immunoblots of ZnT2 and LAMP1 (lysosomal marker) and (E) zinc concentration in lysosome-enriched fractions isolated from MGs from lean lactating and obese lactating mice. Zinc concentration data are means \pm SDs, $n = 5$ mice/group. * $P = 0.05$. LAMP1, lysosome-associated membrane protein 1; LC3, microtubule-associated protein light chain 3; MG, mammary gland; MW, molecular weight; v-ATPase, vacuolar-type H⁺-ATPase; ZnT2, zinc transporter 2.

and p-STAT3 as markers of apoptosis and involution, respectively, by immunoblotting. Indeed, we found that caspase-3 expression was greater in MGs from obese lactating mice than in MGs from lean lactating mice (Figure 5A; $P = 0.05$), which paralleled the presence of apoptotic cells shed into the alveoli lumen in obese lactating mice (Figure 5B). Importantly, MGs of obese lactating mice had a significantly greater ratio of p-STAT3:t-STAT3 compared with lean lactating mice (Figure 5C; $P < 0.01$). Collectively, our study suggests that lactation defects in obese mice are associated with a redistribution of intracellular zinc pools and the activation of cell death of MECs and premature involution.

Discussion

Consistent with previous reports (5, 31, 32), we found that diet-induced obesity in mice created a proinflammatory microenvironment in the MG, including increased adipocytes, macrophage infiltration, and proinflammatory cytokines, which was associ-

ated with an increased rate of lactation failure. The relevance of this observation reflects the fact that optimal lactation is supported by anti-inflammatory T helper type 2 cytokines (e.g., IL-4, IL-13, and IL-5) (37) and that there is a “spike” in proinflammatory cytokines and immune cell mediators at the onset of involution (38). Importantly, to our knowledge, our data show for the first time that the proinflammatory microenvironment of the obese MG during lactation is associated with a redistribution of subcellular zinc pools, suppression of ER stress and enhanced autophagy, and the activation of premature involution.

The metabolic demands of lactation normally result in ER stress and the UPR, which upregulates genes in the secretory pathway (39) to manage the massive influx of milk proteins and lipids. Here, we provide the novel demonstration that when the inherent ER stress of lactation is compounded by the pathophysiologic ER stress of obesity (11), the UPR is suppressed, which is associated with defects in protein secretion and the activation of premature involution (10). Moreover, we provide

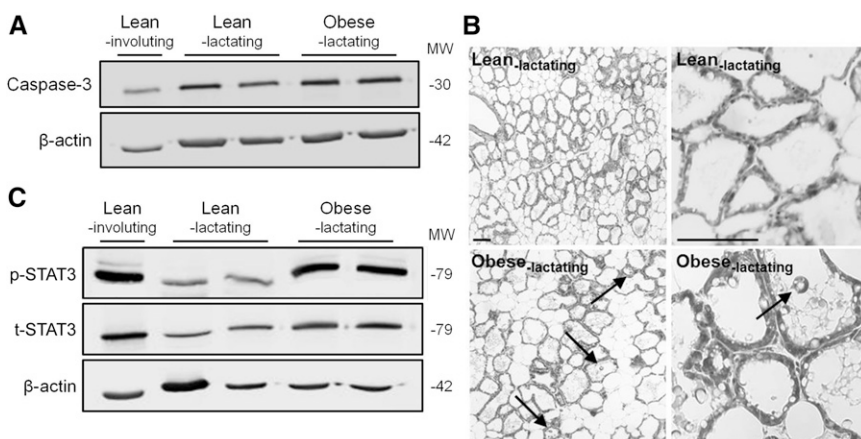


FIGURE 5 Markers of cell death and involution in MGs from lean lactating and obese lactating mice. (A) Representative immunoblots of protein abundance of caspase-3. Involuting MGs from lean mice are shown for comparison. β -Actin was used as a loading control. (B) H&E-stained MG sections from lean lactating and obese lactating mice at low (left) and high (right) magnification. Arrows point to apoptotic cells shed into the lumen (scale bars = 100 μ m). (C) Representative immunoblot of protein abundance of p-STAT3 and t-STAT3. Involuting MGs from lean mice are shown for comparison. H&E, hematoxylin and eosin; MG, mammary gland; MW, molecular weight; p-STAT3, phosphorylated signal transducer and activator of transcription 3; t-STAT3, total signal transducer and activator of transcription 3.

novel evidence that this effect is associated with alterations in ER zinc management. Others have shown that zinc is required in the ER as a cofactor for many different proteins that function in quality-control mechanisms (18, 40, 41) and that low zinc in the ER (18–20) upregulates UPR target genes such as karyogamy 2 (*KAR2*), the yeast homolog of the mammalian *HSPA5* gene (18), and inositol-requiring 1 (*IRE1*) (42), activating ER stress. Consistent with reports in other systems (21, 43), our data suggest that attenuation of ZIP7-mediated zinc release may be an important component in ER zinc management and the suppression of ER stress in the MGs of obese mice and the activation of involution. However, whether the suppression in the UPR was a result of premature activation of remodeling mechanisms or was responsible for premature involution is not currently understood. Another novel finding from our study is that TNF suppresses ZIP7 and the UPR. However, ER zinc concentration was not affected in TNF-injected mice, suggesting that the suppression in ZIP7 in the complex context of obesity may not be a direct effect of TNF, but rather an indirect effect. Alternatively, the suppression in ZIP7 may be caused by a decrease in the proportion of secretory epithelial cells because of cell death. Regardless, our data suggest that aberrant inflammation in the MGs of obese mice may contribute to the suppression in ER stress and decreased secretory capacity of MECs through zinc-mediated mechanisms.

Emerging data demonstrate that ER stress activates autophagy as a cytoprotective mechanism (13) and thus protects the integrity of the lactating MG. The induction of autophagy by ER stress serves multiple purposes. First, it provides a means for unfolded proteins that escape ER-associated degradation to be sent to lysosomes or vacuoles for degradation (44) and, second, it maintains energy homeostasis to curb cell death (45). Moreover, recent evidence suggests that increased autophagy in the involuting MG functions to mediate dead cell clearance (35). However, sustained autophagy can lead to cell death (46). In the present study, we found increased lysosomal zinc content in the MGs of obese mice, which was associated with increased lysosomal activity and augmented autophagy. Many reports show that zinc is an underlying regulator of lysosomal activity and autophagy [reviewed by Lee and Koh (15)]. Moreover, we recently demonstrated that TNF stimulates ZnT2-mediated zinc accumulation in lysosomes, which is required for increased lysosomal activity in MECs during involution (9). This suggests that the augmented production of TNF in the obese MG microenvironment may drive ZnT2-mediated zinc accumulation in lysosomes, increasing lysosomal activity and autophagy. However, sustained autophagy can induce cell death after lysosomal membrane permeabilization and the release of lysosomal proteases. Collectively, this suggests that obesity-induced inflammation may alter subcellular zinc pools, affecting ER stress, autophagy, and cell death of MECs, resulting in premature involution and impaired secretory capacity.

Ultimately, our study illustrates that during lactation, the added pathophysiologic ER stress associated with obesity tips the phenotype toward cell death, predisposing MGs in obese mice toward lactation failure. Because we find increased lysosomal activity and autophagy, the suppression in ER stress is likely a result of feedback, because of the activation of remodeling mechanisms in the obese MG. Importantly, our mechanistic studies provide a novel association between obesity-induced inflammation, altered subcellular zinc pools, and the activation of premature MG involution. Consistent with our results, others have demonstrated that obesity-induced MG inflammation is reversed in response to caloric restriction (47).

Future studies should determine whether resolution of inflammation before or during pregnancy is an effective strategy to increase the likelihood of lactation success.

Acknowledgments

VV and SLK conceived the study; SRH, VV, and SLK designed the experiments and analyzed the data; SRH and VV conducted the experiments; SRH and SLK wrote the manuscript; SLK had primary responsibility for final content. All authors read and approved the final manuscript.

References

1. Flegal KM, Carroll MD, Ogden CL, Curtin LR. Prevalence and trends in obesity among US adults, 1999–2008. *JAMA* 2010;303:235–41.
2. Jevitt C, Hernandez I, Groer M. Lactation complicated by overweight and obesity: supporting the mother and newborn. *J Midwifery Womens Health* 2007;52:606–13.
3. Rasmussen KM. Association of maternal obesity before conception with poor lactation performance. *Annu Rev Nutr* 2007;27:103–21.
4. Stuebe AM, Horton BJ, Chetwynd E, Watkins S, Grewen K, Meltzer-Brody S. Prevalence and risk factors for early, undesired weaning attributed to lactation dysfunction. *J Womens Health (Larchmt)* 2014;23:404–12.
5. Hernandez LL, Grayson BE, Yadav E, Seeley RJ, Horseman ND. High fat diet alters lactation outcomes: possible involvement of inflammatory and serotonergic pathways. *PLoS One* 2012;7:e32598.
6. Wellen KE, Hotamisligil GS. Obesity-induced inflammatory changes in adipose tissue. *J Clin Invest* 2003;112:1785–8.
7. Zeyda M, Stulnig TM. Adipose tissue macrophages. *Immunol Lett* 2007;112:61–7.
8. Levy CS, Slomiansky V, Gattelli A, Nahmod K, Pelisch F, Blaustein M, Srebrow A, Coso OA, Kordon EC. Tumor necrosis factor alpha induces LIF expression through ERK1/2 activation in mammary epithelial cells. *J Cell Biochem* 2010;110:857–65.
9. Hennigar SR, Seo YA, Sharma S, Soybel DI, Kelleher SL. ZnT2 is a critical mediator of lysosomal-mediated cell death during early mammary gland involution. *Sci Rep* 2015;5:8033.
10. Gregor MF, Misch ES, Yang L, Hummasti S, Inouye KE, Lee AH, Bierie B, Hotamisligil GS. The role of adipocyte XBP1 in metabolic regulation during lactation. *Cell Reports* 2013;3:1430–9.
11. Ozcan U, Cao Q, Yilmaz E, Lee AH, Iwakoshi NN, Ozdelen E, Tuncman G, Görgün C, Glimcher LH, Hotamisligil GS. Endoplasmic reticulum stress links obesity, insulin action, and type 2 diabetes. *Science* 2004;306:457–61.
12. Lee GH, Kim DS, Kim HT, Lee JW, Chung CH, Ahn T, Lim JM, Kim IK, Chae HJ, Kim HR. Enhanced lysosomal activity is involved in Bax inhibitor-1-induced regulation of the endoplasmic reticulum (ER) stress response and cell death against ER stress: involvement of vacuolar H⁺-ATPase (V-ATPase). *J Biol Chem* 2011;286:24743–53.
13. Ogata M, Hino S, Saito A, Morikawa K, Kondo S, Kanemoto S, Murakami T, Taniguchi M, Tani I, Yoshinaga K, et al. Autophagy is activated for cell survival after endoplasmic reticulum stress. *Mol Cell Biol* 2006;26:9220–31.
14. Lin JH, Li H, Yasumura D, Cohen HR, Zhang C, Panning B, Shokat KM, Lavail MM, Walter P. IRE1 signaling affects cell fate during the unfolded protein response. *Science* 2007;318:944–9.
15. Lee SJ, Koh JY. Roles of zinc and metallothionein-3 in oxidative stress-induced lysosomal dysfunction, cell death, and autophagy in neurons and astrocytes. *Mol Brain* 2010;3:30.
16. Lopez V, Kelleher SL. Zinc transporter-2 (ZnT2) variants are localized to distinct subcellular compartments and functionally transport zinc. *Biochem J* 2009;422:43–52.
17. McCormick N, Velasquez V, Finney L, Vogt S, Kelleher SL. X-ray fluorescence microscopy reveals accumulation and secretion of discrete intracellular zinc pools in the lactating mouse mammary gland. *PLoS One* 2010;5:e11078.
18. Ellis CD, Wang F, MacDiarmid CW, Clark S, Lyons T, Eide DJ. Zinc and the Msc2 zinc transporter protein are required for endoplasmic reticulum function. *J Cell Biol* 2004;166:325–35.

19. Lin W, Buccella D, Lippard SJ. Visualization of peroxynitrite-induced changes of labile Zn²⁺ in the endoplasmic reticulum with benzoefluoranthene-based fluorescent probes. *J Am Chem Soc* 2013;135:13512–20.
20. Jeong J, Walker JM, Wang F, Park JG, Palmer AE, Giunta C, Rohrbach M, Steinmann B, Eide DJ. Promotion of vesicular zinc efflux by ZIP13 and its implications for spondylocheiro dysplastic Ehlers-Danlos syndrome. *Proc Natl Acad Sci USA* 2012;109:E3530–8.
21. Groth C, Sasamura T, Khanna MR, Whitley M, Fortini ME. Protein trafficking abnormalities in *Drosophila* tissues with impaired activity of the ZIP7 zinc transporter Catsup. *Development* 2013;140:3018–27.
22. Ha SK, Kim J, Chae C. Role of AMP-activated protein kinase and adiponectin during development of hepatic steatosis in high-fat diet-induced obesity in rats. *J Comp Pathol* 2011;145:88–94.
23. Van Heek M, Compton DS, France CF, Tedesco RP, Fawzi AB, Graziano MP, Sybertz EJ, Strader CD, Davis HR. Diet-induced obese mice develop peripheral, but not central, resistance to leptin. *J Clin Invest* 1997;99:385–90.
24. Dhar MS, Sommardahl CS, Kirkland T, Nelson S, Donnell R, Johnson DK, Castellani LW. Mice heterozygous for *Atp10c*, a putative amphipath, represent a novel model of obesity and type 2 diabetes. *J Nutr* 2004;134:799–805.
25. Chandarana K, Gelegen C, Karra E, Choudhury AI, Drew ME, Fauveau V, Viollet B, Andreelli F, Withers DJ, Batterham RL. Diet and gastrointestinal bypass-induced weight loss: the roles of ghrelin and peptide YY. *Diabetes* 2011;60:810–8.
26. El-Haschimi K, Lehnert H. Leptin resistance—or why leptin fails to work in obesity. *Exp Clin Endocrinol Diabetes* 2003;111:2–7.
27. Dempsey C, McCormick NH, Croxford TP, Seo YA, Grider A, Kelleher SL. Marginal maternal zinc deficiency in lactating mice reduces secretory capacity and alters milk composition. *J Nutr* 2012;142:655–60.
28. Kelleher SL, Lonnerdal B. Zinc transporters in the rat mammary gland respond to marginal zinc and vitamin A intakes during lactation. *J Nutr* 2002;132:3280–5.
29. Kelleher SL, Lonnerdal B. Mammary gland copper transport is stimulated by prolactin through alterations in *Ctr1* and *Atp7A* localization. *Am J Physiol Regul Integr Comp Physiol* 2006;291:R1181–91.
30. Lodish HF. *Molecular cell biology*. 6th ed. New York: W.H. Freeman; 2008.
31. Kamikawa A, Ichii O, Yamaji D, Imao T, Suzuki C, Okamatsu-Ogura Y, Terao A, Kon Y, Kimura K. Diet-induced obesity disrupts ductal development in the mammary glands of nonpregnant mice. *Dev Dyn* 2009;238:1092–9.
32. Subbaramaiah K, Howe LR, Bhardwaj P, Du B, Gravaghi C, Yantiss RK, Zhou XK, Blaho VA, Hla T, Yang P, et al. Obesity is associated with inflammation and elevated aromatase expression in the mouse mammary gland. *Cancer Prev Res (Phila)* 2011;4:329–46.
33. Helminen HJ, Ericsson JL. Quantitation of lysosomal enzyme changes during enforced mammary gland involution. *Exp Cell Res* 1970;60:419–26.
34. Mijaljica D, Prescott M, Devenish RJ. V-ATPase engagement in autophagic processes. *Autophagy* 2011;7:666–8.
35. Teplova I, Lozy F, Price S, Singh S, Barnard N, Cardiff RD, Birge RB, Karantzis V. ATG proteins mediate efferocytosis and suppress inflammation in mammary involution. *Autophagy* 2013;9:459–75.
36. Dong H, Czaja MJ. Regulation of lipid droplets by autophagy. *Trends Endocrinol Metab* 2011;22:234–40.
37. Khaled WT, Read EK, Nicholson SE, Baxter FO, Brennan AJ, Came PJ, Sprigg N, McKenzie AN, Watson CJ. The IL-4/IL-13/Stat6 signalling pathway promotes luminal mammary epithelial cell development. *Development* 2007;134:2739–50.
38. Clarkson RW, Wayland MT, Lee J, Freeman T, Watson CJ. Gene expression profiling of mammary gland development reveals putative roles for death receptors and immune mediators in post-lactational regression. *Breast Cancer Res* 2004;6:R92–109.
39. Travers KJ, Patil CK, Wodicka L, Lockhart DJ, Weissman JS, Walter P. Functional and genomic analyses reveal an essential coordination between the unfolded protein response and ER-associated degradation. *Cell* 2000;101:249–58.
40. Mann KJ, Seveler D. 1,10-Phenanthroline inhibits glycosylphosphatidylinositol anchoring by preventing phosphoethanolamine addition to glycosylphosphatidylinositol anchor precursors. *Biochemistry* 2001;40:1205–13.
41. Tang W, Wang CC. Zinc fingers and thiol-disulfide oxidoreductase activities of chaperone DnaJ. *Biochemistry* 2001;40:14985–94.
42. Nguyen TS, Kohno K, Kimata Y. Zinc depletion activates the endoplasmic reticulum-stress sensor *Ire1* via pleiotropic mechanisms. *Biosci Biotechnol Biochem* 2013;77:1337–9.
43. Kelleher SL, Velasquez V, Croxford TP, McCormick NH, Lopez V, Macdavid J. Mapping the zinc-transporting system in mammary cells: molecular analysis reveals a phenotype-dependent zinc-transporting network during lactation. *J Cell Physiol* 2012;227:1761–70.
44. Arvan P, Zhao X, Ramos-Castaneda J, Chang A. Secretory pathway quality control operating in Golgi, plasmalemmal, and endosomal systems. *Traffic* 2002;3:771–80.
45. Levine B, Yuan J. Autophagy in cell death: an innocent convict? *J Clin Invest* 2005;115:2679–88.
46. Kroemer G, Jäättelä M. Lysosomes and autophagy in cell death control. *Nat Rev Cancer* 2005;5:886–97.
47. Bhardwaj P, Du B, Zhou XK, Sue E, Harbus MD, Falcone DJ, Giri D, Hudis CA, Kopelovich L, Subbaramaiah K, et al. Caloric restriction reverses obesity-induced mammary gland inflammation in mice. *Cancer Prev Res (Phila)* 2013;6:282–9.